

# DEVELOPMENT OF NEW IN-MILL MECHANICAL TESTING TOWARDS X100 ASSESSMENT FOR GAS PIPE

Gilles Perrin<sup>#</sup>, Michaël Martinez, Pierre Odru - Institut Français du Pétrole, France  
Trung T. Luu<sup>\*</sup>, André Pineau, Benoît Tanguy, Jacques Besson - Ecole des Mines de Paris, France

## ABSTRACT

This paper presents the early results of a 2003-2009 research program aiming at using X100 steel for gas pipelines, through controlling axial crack propagation hazard. For such high resistance steels, classical correlation between Charpy tests and scale 1 burst tests fall apart. This is due to complicate, tilted geometry of the fracture plane in scale 1 tests. A way of bridging between mill acceptance tests and field situation is proposed. It includes material testing, Gurson based fracture model development, and three-dimensional (3D) Finite Element Method (FEM) simulations. Results are implemented in ZEBULON and ABAQUS commercial FEM codes.

## KEYWORDS

Gas; Pipeline; X100; Steel; Axial; Fracture; Acceptance; Test; FEM; Computation.

## INTRODUCTION

Economic gas transportation on long distance requires the use of high pressure and high grade steel. In the recent years, steel pipe manufacturers have begun to offer thick steel plates of high yield strength which can be formed into large diameter tubes: grade X90 through X120 steels are indeed obtained thanks to Thermo-Mechanical Controlled Process (TMCP). The present paper is concerned mainly with X100 grade.

This paper addresses:

- (i) the issue of fast ductile axial fracture in a gas transportation pipeline, classically aside from the axial welds;
- (ii) the propagation and arrest of an axial crack;
- (iii) the strategy to design an in-mill acceptance test for steel, regarding its fracture arrest capabilities, adequate for grade X100.

---

<sup>#</sup> Corresponding author – E-mail : gilles.perrin@ifp.fr

<sup>\*</sup> Also with Institut Français du Pétrole

It should be noted that the issue under concern is one of the few issues which at the present time forbid standardization of X100 steel for large diameter (e.g. 1422 mm = 56"), high thickness (e.g. 25 mm), used for 200 bar (approximate) gas transportation.

The present paper reports early results of a project aimed at answering these questions. Considering the necessity of standardizing a qualified acceptance test in order to install X100 gas pipes, it appears :

- (a) such an acceptance test must be qualified,
- (b) a specimen geometry and load must be defined,
- (c) a simulation tool for specimen fracture is necessary for pre-screening of point (b) above,
- (d) a simulation tool which bridges between different scales is to be built.

Accordingly is the project compound of 4 tasks:

- (A) Build a fracture computational simulation tool.
- (B) Use this tool to determine a preliminary acceptance test geometry and load.
- (C) Run experimental program to qualify the acceptance test.
- (D) Standardize the acceptance test for industrial use.

Chart of task (A) and its output is presented on Figure 1.

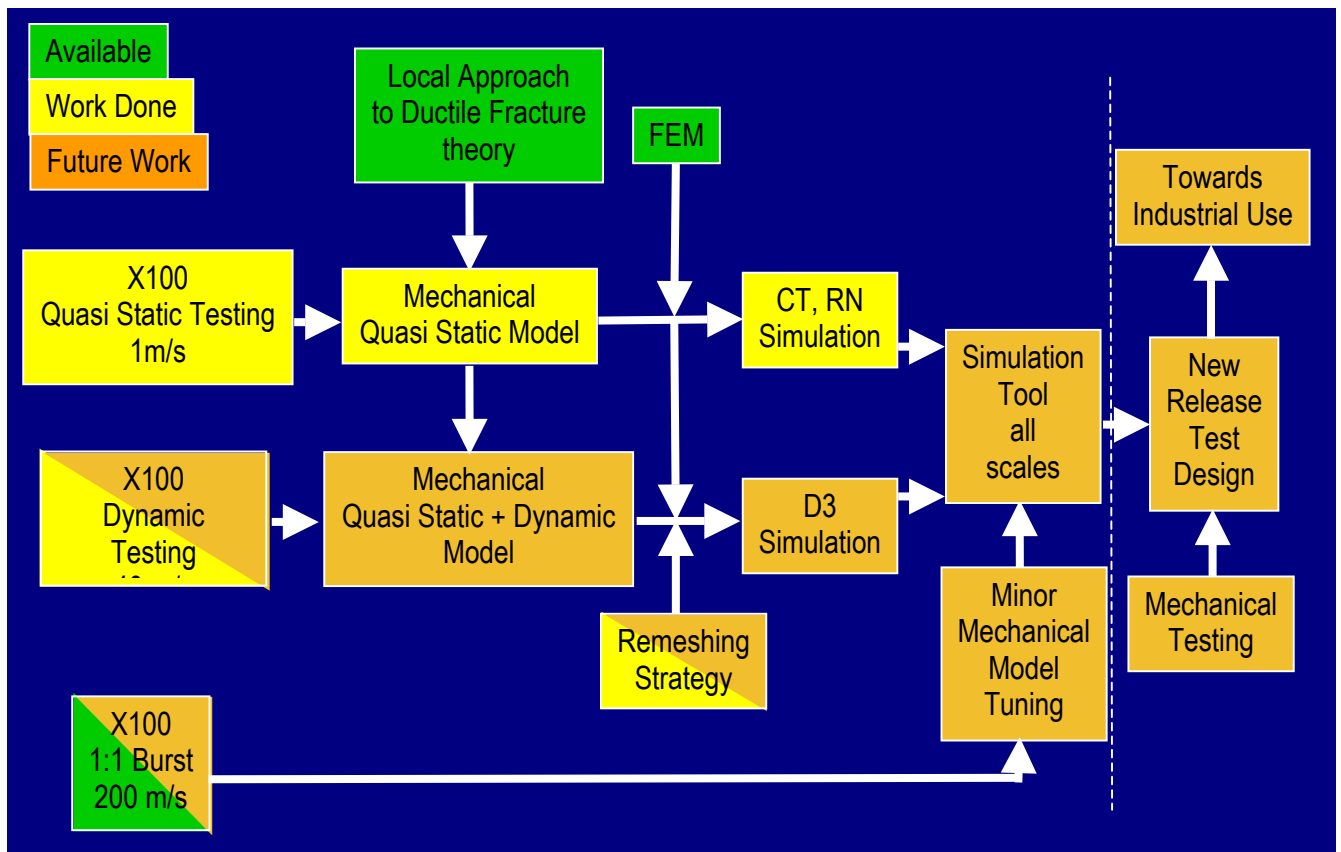


Fig. 1: Chart of task (A) (left of interrupted line) and its output. Items coloured in green are elements already known prior to the present study. Items in yellow are points which are realized today. Items in orange are to be done in forthcoming work.

This paper is mainly concerned with determination of X100 constitutive equations, small-scale and dynamic, intermediate scale testing. It is organized as follows. Section 1 recalls the reasons why the

acceptance tests classically used for lower grades appear to be inadequate for grade X100. Section 2 addresses the fitting of anisotropic elastoplastic constitutive equations for X100. To address ductile fracture of X100, it is relevant to resort to local approach to ductile fracture theory. Essential features of this theory, including the well-known pertinent damage parameter, local void volume fraction within the steel, is presented in Section 3. Tuning of these models to adequately predict axial failure needs an appropriate testing program on both small scale specimens and large scale specimens. Section 4 is devoted to presenting small scale testing and subsequent model fitting. In order to extend the model obtained to larger crack velocity, it is resorted to large scale testing, which allows crack velocity range as high as 40 m/s ; this is reported in Section 5. Next, Section 6 mentions the difficulties of long running crack computational simulations and the remeshing solutions which are prepared. Finally, perspectives for future work and project completion are presented in the conclusion.

## 1. STATE OF THE ART

### Acceptance tests and their use

Classically, the Charpy V Notch test (CVN) is used to qualify a pipe regarding crack failure risk. The energy lost by the Charpy pendulum after specimen rupture, named Charpy V-Notch energy or simply CVN, is compared to a "required CVN". The pipe destination enters the definition of the latter criterion, through the use of formulae which account for numerous parameters such as: pipe diameter and thickness, steel material parameters, gas pressure. A number of such formulae or algorithms, for example the Battelle Two Curve approach (see e.g. Maxey [9] ), coexist, at least for grades lower than X70.

For grades X70 and higher, though, Buzzichelli [3] has shown that correlation between the extrapolated Battelle Two Curve approach prediction method and actual CVN measures display a scatter ranging from 1 to 1.26. This justifies the need for a new acceptance test. To that aim, an effort to characterize axial fracture was undertaken and the early results are presented here.

### Tracks to improve correlation between mill-scale assessment tests and full field experiments

This study was performed on an X100 steel developed by EUROPIPE. Its chemical composition is given in Table 1.

Table 1: Chemical composition of grade X100 steel studied (wt%).

C	Mn	Si	P	S	Al	Ti	B
0.063	1.807	0.349	0.013	6ppm	0.029	0.018	0.006
Ni	Cr	Cu	Mo	Nb	V	Ca	N
0.25	0.034	0.021	0.282	0.04	0.006	0.023	0.005

Laboratory tests on small scale smooth tensile specimens show ovalisation of the fracture necking (Perrin et al. [12], Luu [7]), as can be seen on Figure 2. The large oval on that Figure is the result of the necking of initially circular specimen cross section. The small, inner oval is the flat region of the ductile crack, germinating and growing from the centre, due to necking. Between the two ovals is the cup and cone tilted ductile fracture zone. This evidences the anisotropy of the steel behaviour.

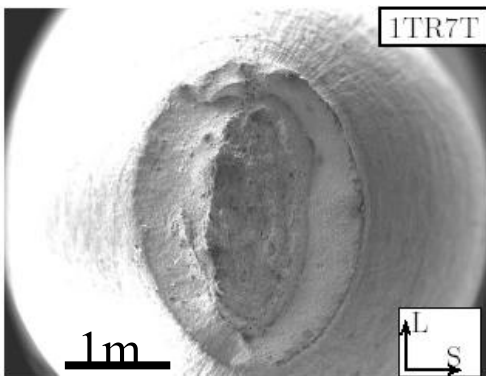


Fig. 2: Specimen after traction rupture in the transverse rolling direction. Directions L and S indicate respectively long and short rolling directions.

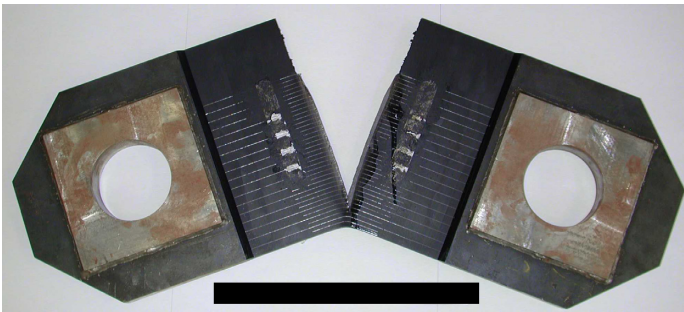


Fig. 3: Large plate (685 mm x 250 mm x 20 mm) subjected to traction causes non flat propagation, and then in crack arrest. Scale bar is 300 mm long.

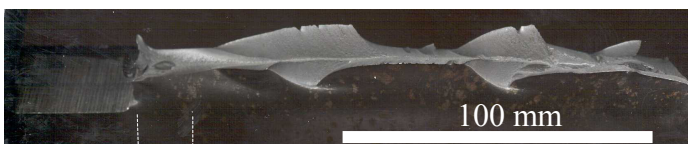


Fig. 4: View from  $\frac{3}{4}$  angle of the facies caused by the fracture of a specimen similar to that shown on Figure 3. Flat initiation zone length is indicated by the interrupted lines.

It is believed that this anisotropy can favour crack propagation instability, and drive the crack into a jigsaw, non planar path out of its initial plane, as evidenced on the 685 mm x 250 mm x 20 mm large specimen shown on Figure 3.

Indeed, Figure 4 shows the facies of a specimen similar to that shown on Figure 3. It is noticeable that the facies is by no means flat, except in a small initiation, centimetre-size zone on the left end side. On the right of this zone, crack bifurcates, tilting alternatively at about  $+45^\circ$  or  $-45^\circ$ . It should be noticed that medium-range (20 m/s) crack propagation velocity is important to obtain this kind of tortured facies.

It is well known that crack tilting leads to apparent toughness increase: it is the reason why Compact Tension toughness measurement specimens should not be thinner than some required value.

Hence, observation of these facies is quite convincing that crack tilting understanding is a key issue to bridge between mill-scale specimen and scale 1 burst tests.

For that reason also, a purely two-dimensional analysis like those performed on lower grade steel (see eg. Kanninen et al. [5]), seems inadequate.

## 2. CONSTITUTIVE EQUATION

Because anisotropy is well known to influence fracture, it was given great attention in determination of constitutive equations for X100. Material behavior was investigated using several specimen geometries: smooth tensile (ST) and notched tensile (NT) with different notch radii. Tensile tests were conducted along long (L), transverse (T) and short (S) directions to characterize the anisotropy of the material. Tensile properties (yield strength at 0.2% plastic strain (YS), ultimate yield strength (UTS) and uniform elongation (UE)) for X100 dedicated plate along three directions are reported on Table 2.

Table 2: X100 dedicated steel plate mechanical properties

Loading direction	YS (MPa)	UTS (MPa)	UE (%)
Long	574	770	7,8
Transverse	614	797	6,6
Short	606	759	6,1

The anisotropic elastoplastic behavior was very well accounted for by a particular case of the model proposed by Bron and Besson [2] (namely choosing  $a = b^1 = b^2$  following the notations of these authors). It is defined by an equivalent stress,  $\sigma_{eq}$ , given by the following equations:

$$\sigma_{eq} = (\alpha\Psi^1 + (1 - \alpha)\Psi^2)^{1/a} \quad (1)$$

$$\Psi^1 = \frac{1}{2} \left( |S_2^1 - S_3^1|^a + |S_3^1 - S_1^1|^a + |S_1^1 - S_2^1|^a \right) \quad (2)$$

$$\Psi^2 = \frac{3^a}{2^a + 2} \left( |S_1^2|^a + |S_2^2|^a + |S_3^2|^a \right) \quad (3)$$

and for  $k = 1, 2$ ,  $S_{i=1,3}^k$  are the principal values of some two stress deviators  $\underline{s}^k$ ,  $k = 1, 2$  defined as follows:

$$s_{11}^k = \frac{(c_2^k + c_3^k)\sigma_{11} - c_2^k\sigma_{22} - c_3^k\sigma_{33}}{3}, \quad s_{12}^k = c_4^k\sigma_{12}, \quad (4)$$

$$s_{22}^k = \frac{(c_3^k + c_1^k)\sigma_{22} - c_3^k\sigma_{33} - c_1^k\sigma_{11}}{3}, \quad s_{13}^k = c_5^k\sigma_{13}, \quad (5)$$

$$s_{33}^k = \frac{(c_1^k + c_2^k)\sigma_{33} - c_1^k\sigma_{11} - c_2^k\sigma_{22}}{3}, \quad s_{23}^k = c_6^k\sigma_{23}. \quad (6)$$

The  $\alpha$ ,  $a$  and  $c_{i=1,\dots,6}^{k=1,2}$  are 14 model parameters. Note that classical Von Mises criterion is retrieved for  $\alpha = 0$ ,  $a = 2$  and  $c_{i=1,\dots,6}^{k=1,2} = 0$ ; Tresca criterion for  $\alpha = 1$ ,  $a = \infty$  and  $c_{i=1,\dots,6}^{k=1,2} = 0$ .

The flow potential  $\phi$  is then defined as:

$$\phi = \sigma_{eq} - R(p) \quad (7)$$

where  $p$  is the equivalent plastic strain,  $R$  is the flow stress and is given by:

$$R(p) = R_0 \left\{ 1 + Q_1 (1 - e^{-k_1 p}) + Q_2 (1 - e^{-k_2 p}) \right\} \quad (8)$$

Using normality flow rule, the direction of plastic strain rate is perpendicular to the yield surface, oriented outwards. It is given by:

$$\underline{\dot{\epsilon}}_p = \dot{\lambda} \frac{\partial \sigma_{eq}}{\partial \underline{\sigma}} \quad (9)$$

where  $\dot{\lambda} > 0$  is the plastic multiplier. The value of effective strain rate stems from the consistency equation which reads in the present framework:

$$\dot{\sigma}_{eq} = \frac{\partial R}{\partial p} \dot{p}. \quad (10)$$

### Determination of the model parameters

Use of this model requires the determination of several unknown material parameters related to hardening and anisotropic behaviour. These parameters have been identified using a three step identification procedure. Firstly, the elastic properties were assumed to be isotropic. A mean value  $E = 210$  MPa was obtained. Secondly, plastic hardening (Eq. 8) is determined supposing a test isotropic material (that is with all  $c_{i=1,\dots,6}^{k=1,2} = 1$ ), but with a specific yield strength for each L, T and S directions: more precisely,  $R_0$  is successively replaced by  $R_0^L$ ,  $R_0^T$  and  $R_0^S$  in equation (8), where  $Q_1, k_1$  represent the plastic hardening for the plastic strain smaller than maximal uniform elongation and are identified on smooth tensile tests. For larger plastic strain, finite element simulations of smooth tensile tests were performed, and  $Q_2, k_2$  were obtained by comparison between simulation

and experiments. In the fitting computations, the isotropic von Mises material yield strength was, for each load direction:  $R_0^L = 572$ ,  $R_0^T = 610$  and  $R_0^S = 572$  MPa.

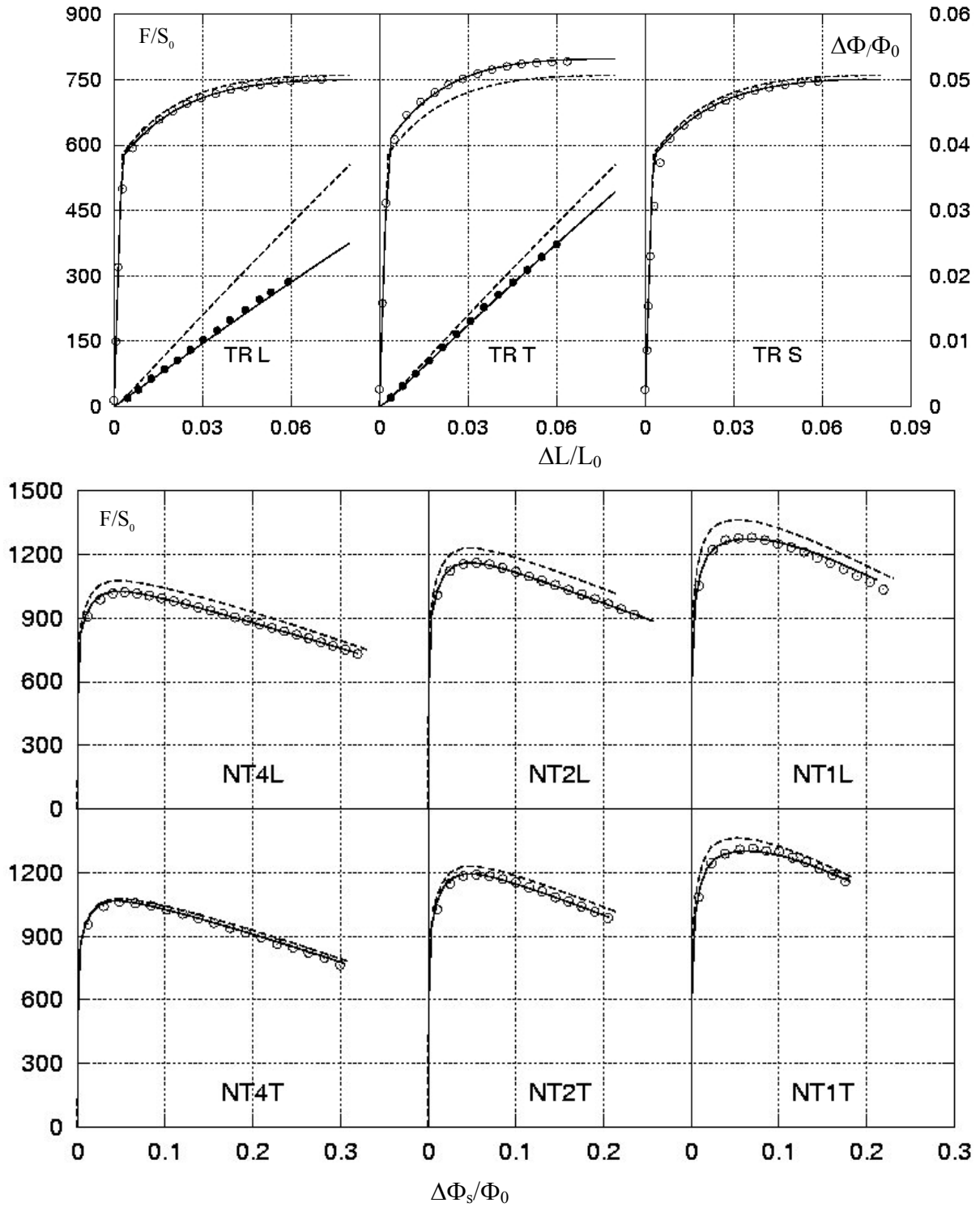


Fig. 5: Comparison between experiments (symbols), von Mises simulations with different  $R_0^L, R_0^T$  and  $R_0^S$  (dashed lines) and simulations with the anisotropic model (solid lines).  $F$  stands for the load and  $S_0$  for the initial cross section. The unit of  $F/S_0$  is MPa (left scale, empty circles). Longitudinal deformation is noted  $\Delta L/L_0$  (loading direction), transverse deformation ( $90^\circ$  from the loading direction, right scale, black dots) is noted  $\Delta \Phi/\Phi_0$  and normalized radial displacement along the short direction in the notch is noted  $\Delta_s \Phi/\Phi_0$ .

In order to account properly for anisotropy, parameter  $R_0$  (Eq. 8) was fixed as the average of the above three yield strength values ( $R_0^L, R_0^T, R_0^S$ ), and parameters  $a, \alpha, c_{1-6}^{1-2}$  were fitted from smooth tensile and notched tensile specimen testing. More precisely, in order to determine accurately the parameters  $c_{1-3}^{1-2}$ , the Lankford coefficients were measured using interrupted smooth tensile test. Other coefficients were adjusted from notched tensile specimen tests.

The fitted parameter values are presented in Table 3 below. Figure 1 shows the comparisons between experiments, the anisotropic model and von Mises criterion.

Table 3: Model parameters of the X100 steel plate

$E$ (GPa)	$\nu$	$R_0$ (Mpa)	$Q_1$	$k_1$	$Q_2$	$K_2$
210	0.3	580	0.367	46.84	1.119	0.741
			$a$	$\alpha$		
			9.25	0.7		
$c_1^1$	$c_2^1$	$c_3^1$	$c_4^1$	$c_5^1$	$c_6^1$	
1.022	1.009	0.961	1.140	1.116	1.118	
$c_1^2$	$c_2^2$	$c_3^2$	$c_4^2$	$c_5^2$	$c_6^2$	
1.572	0.442	0.536	-0.014	0.924	1.183	

Such a precise knowledge of steel behaviour allows to study its fracture in good conditions.

### 3. LOCAL APPROACH TO DUCTILE FRACTURE

#### Description of the approach under construction

Same phenomena govern centimetre scale rupture with crack velocity around 2 m/s (Figure 2), decimetre scale rupture with crack velocity around 20 m/s (Figures 3 and 4) and scale 1 burst tests scale rupture with crack velocity around 200 m/s. These phenomena are:

- (i) damage process that causes local ruin of the material;
- (ii) anisotropic elasto-plastic behaviour of the material;
- (iii) non homogeneous effects of mill thermo-mechanical history;
- (iv) influence of crack velocity on the material behaviour;
- (v) influence of thermal softening due to crack tip heat dissipation on the material behaviour.

In order to clarify point (i), a major amount of work has been done since the early 1960's to understand ductile fracture as a local three stage process. Mc Clintock [10] provides a review of this period.

To understand the first stage, one must consider pre-existing inclusions in the material, be they small as in the case of the X100 steel under study: Figure 6 shows a 5 micron diameter inclusion in the ferrite matrix.

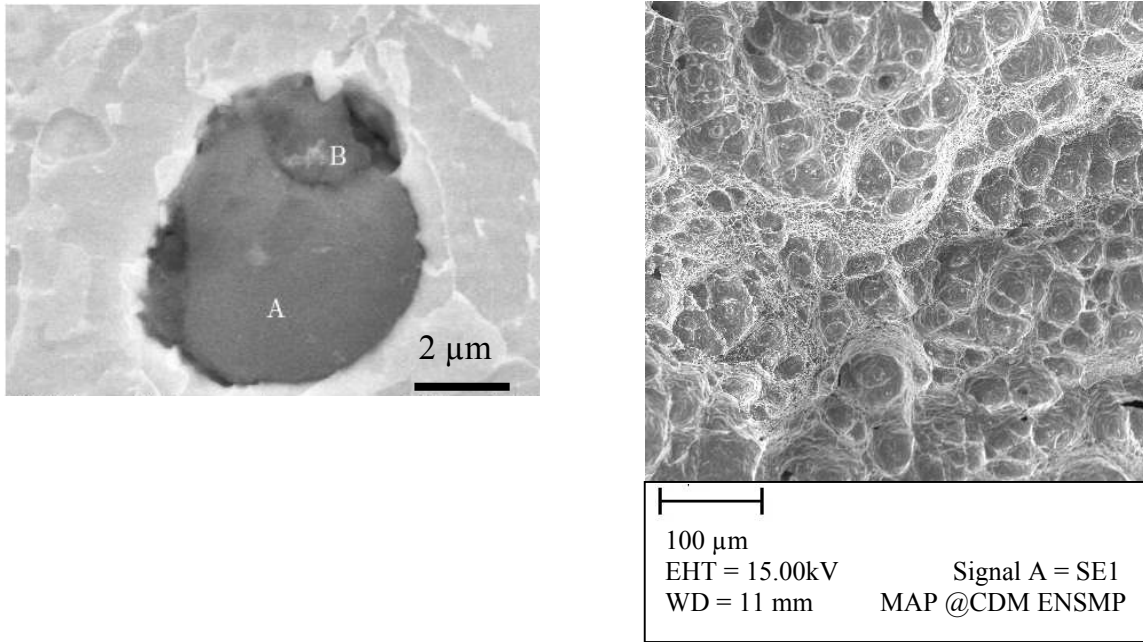


Fig. 6: SEM examination of an initial inclusion (left) and final fracture facies (right). Left view shows a multiphase micron size inclusion compound of aluminium oxide (A) and calcium sulphide (B) representative of inclusions present in the X100 steel under study. On the right is a representative top view of cavities which have, firstly, considerably grown (volume ratio 1 to about 1000) and secondly coalesced.

For a number of materials, including grade X100 steel, once local stresses exceed some level, inclusions break apart or disbond from the metal matrix around them. Numerous voids throughout the material hence appear: they can be observed through microscopic examination. At that stage, an important parameter comes in: the average value of porosity (or void volume fraction)  $f$  on a local volume  $V$  of material, this volume being of the order of a few ferrite grains, depending on the material:

$$f \equiv \frac{\text{Total volume of voids in volume } V}{V} \tag{11}$$

It appears that porosity  $f$ , together with volume scale  $V$  at which it is measured are the paramount parameters to explain ductile fracture. The reason has been made clear by Gurson [4]. A thick-walled hollow sphere made of an ideally plastic matrix is evidently a good Representative Volume Element (RVE) for ductile fracture. Gurson [4] shows that the yield function of this RVE is very close to analytic expression:

$$\Phi\left(\sigma_m, \sigma_{eq}\right) \equiv \left(\frac{\sigma_{eq}}{\sigma_0}\right)^2 + 2f \cosh\frac{3\sigma_m}{2\sigma_0} - 1 - f^2 \leq 0, \quad (12)$$

where  $\sigma_m = \frac{1}{3}(\sigma_{11} + \sigma_{22} + \sigma_{33})$  denotes the first invariant of the stress tensor,  $\sigma_{eq}$  denotes the Von Mises equivalent strain and  $\sigma_0$  denotes the yield stress of the matrix

The Gurson model presented above is theoretically established, on the basis of simplified physical assumptions. Yet, further literature (see e.g. Marini et al. [8], Becker et al. [1], Koplik and Needleman [6]) has demonstrated that introduction of some tuneable parameters makes the model able to represent ductile materials yield locus with a good accuracy, sufficiently to constitute the backbone of a ductile fracture model.

During the second stage of ductile failure void enlargement is observed; it is due to ductile flow of the matrix. It is common sense to understand that void growth lowers the bearing capacity of the material. It is coherent with the observation, that yield locus provided by Gurson model shrinks when porosity grows. A less straightforward characteristic of the Gurson model (and of its tuneable versions) is that it provides an expression of the void growth rate as a function of the mechanical fields (see, for example, Gurson [4]). Figure 6 shows that for the steel under study, void growth is very important : where initial inclusion diameter is around 5  $\mu\text{m}$  (left of Figure 6), final cavities can reach a diameter around 50  $\mu\text{m}$  (left of Figure 6); cavity growth ration is hence around 1000. Void enlargement rate depends also on plastic behaviour of steel matrix: the measures presented in Section 2 are taken into consideration here.

Finally, the third stage of ductile rupture is coalescence of voids into a small crack, which afterwards grows by coalescence of its tip with other voids close to it. In the early modelling, coalescence is considered to occur at loci where and when porosity  $f$  reaches some constant critical value usually denoted  $f_c$ . It is now acknowledged that critical value  $f_c$  is mechanical field dependent.

The point to be made is that a procedure to simulate fracture is made available, at that point. For sure, stresses and strains are not homogeneous in current pieces: Charpy specimens, Compact Tension specimens, large plates shown on Figure 3 or scale 1 burst tests. For that reason, fracture simulation using local approach to fracture are advantageously implemented in Finite Element Method (FEM) computer codes.

This is hence generally agreed to be enough to fulfil a good representation of phenomenon (i) : local damage of the material. Phenomena (ii) to (v) are then accounted for by sophistication of original Gurson model. It is not the locus here to develop thoroughly the literature about establishing tuneable versions of the Gurson model and tuning the parameters to fit actual testing; an example of this and references can be found for instance in Rivalin [13] and [14]. Yet, we explain in the next Sections the most important aspects of the tuning of the parameters of the model, and how it is related to mechanical testing.

#### 4. SMALL SCALE FRACTURE TESTING

This involves specimen with a centimetre-size fracture path. The interest of this testing is to obtain, through a large number of tests, a sufficient amount of information on the elastoplastic behaviour of the material and its fracture parameters. This results firstly in a choice of constitutive equations to represent: elasticity, plastic locus, hardening, plastic anisotropy, cyclic effects. Secondly, fracture parameters are fitted: initial void volume fraction, augmented Gurson model parameters, coalescence criterion and mesh size on the crack path. Note that mesh size being an important parameter seems paradoxical, since one is used to well-posed mathematical problems with convergence to physical solution in the zero mesh size limit. In the present case however, crack simulations do not converge towards any interesting limit when mesh size (more precisely mesh height across the presumed crack plane) tends towards zero. Indeed, it converges to a zero energy fracture mode instead. For that reason, mesh height  $h$  should be chosen of the same order of the average inter cavity distance.

Based on small scale testing on notch tensile specimens, a crack propagation simulation procedure which is sufficient to represent the slow propagating fractures was obtained. It was then used to simulate a Compact Tension test, as illustrated on Figures 7 and 8. No fitting was allowed to simulate the CMOD – load curve for CT specimens shown on Figure 8. Comparison shown between 3D computational simulation and test results hence show that the simulation tool is quite robust for different crack geometries.

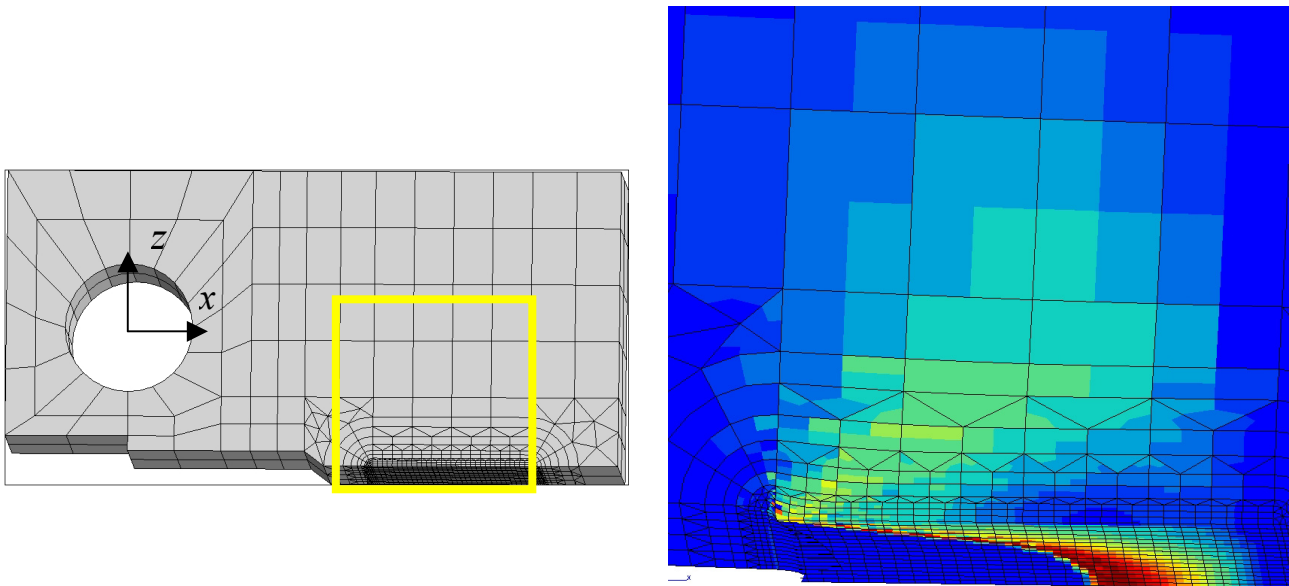


Figure 7: Three dimensional computational simulation of Compact Tension test. Initial mesh of CT specimen is shown on the left. Yellow window highlights the area of interest. Picture on the right shows a zoom of yellow window. Isovalues of stress component  $\sigma_{zz}$  are shown. Colour code is blue for 0 MPa and dark red for 2100 MPa.

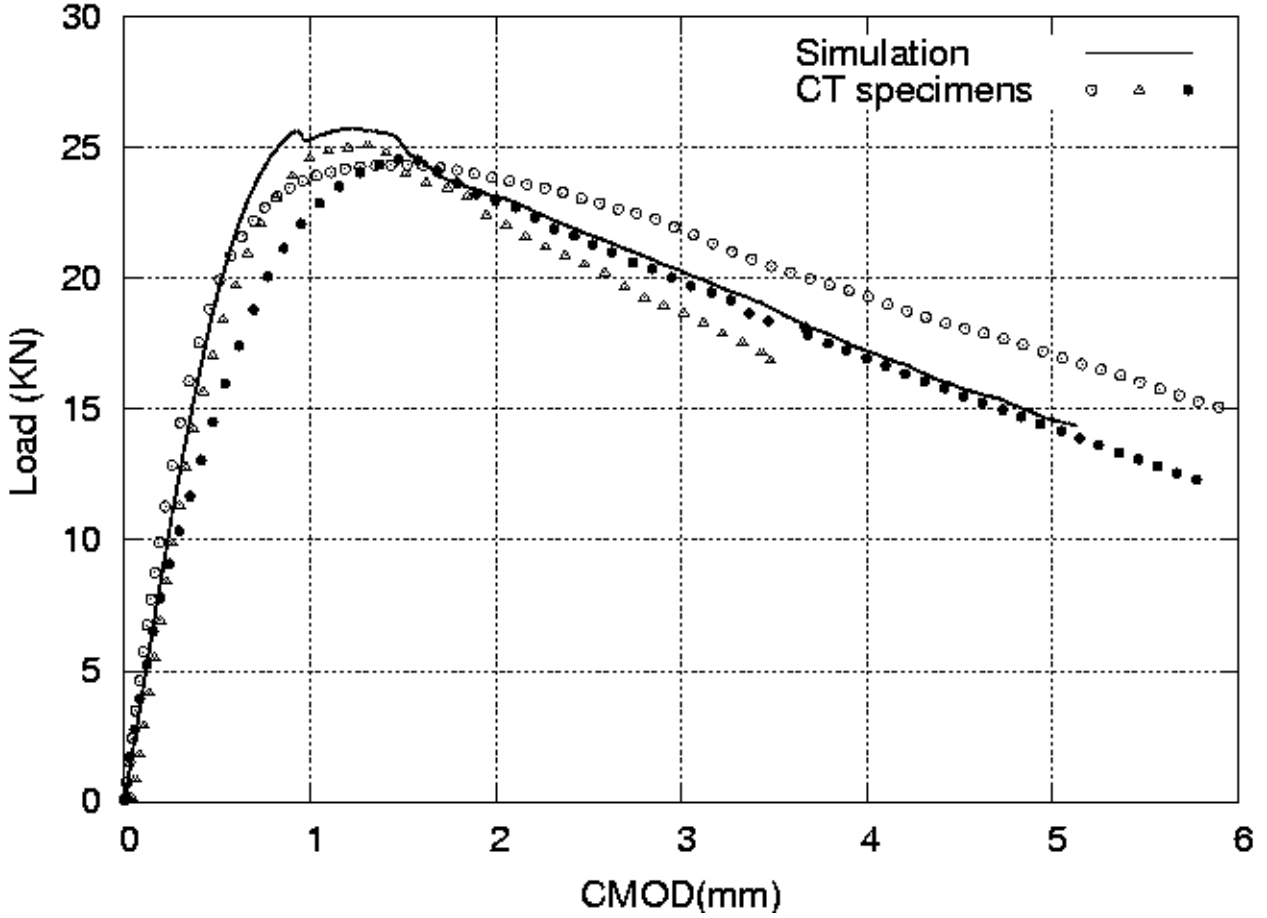


Figure 8: Comparison between computation results (solid line) and three Compact Tension specimen tractions.

Also, CT testing revealed some delaminating during CT tests which results in jogs in the traction curve. This peculiarity is under current study.

## 5. DYNAMIC TESTING

Yet, it is well known that high velocity crack propagation produces heat at the crack tip, and that subsequent temperature rise influences elastoplastic constitutive equations. It appears that this phenomenon cannot be quantified from small scale experiments, because crack velocity, of the order of 2 m/s, is too small.

To reach higher velocities, large plates similar to the torn one presented on Figure 3, are tested using a 4000 kN traction machine with low stiffness (35 kN/mm). Tortured fracture facies are obtained (see Figure 4, or the somewhat simpler one shown on Figure 9). During the test, crack advance  $a(t)$  and velocity and load  $P(t)$  - displacement  $\delta(t)$  curve are monitored. One important data provided by this test is the energy dissipation rate defined as (e.g. [14]):

$$R(t) = \frac{1}{B} \frac{d}{da} \left( \int_0^\delta P(t) d\delta(t) - \frac{1}{2} C(t) P(t)^2 \right), \quad (13)$$

where  $C(t)$  denotes the compliance of the specimen. An example of energy dissipation rate is shown on Figure 10. It may be noted that its value is logically a little lower than that found on X80 grade by Rivalin [13].

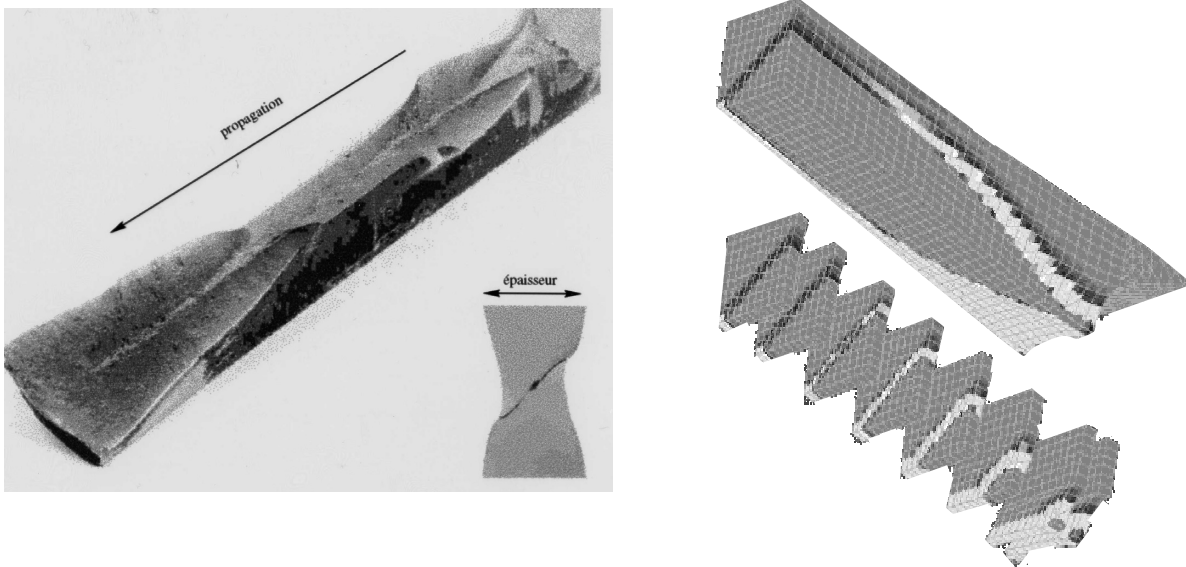


Fig. 9: An example of tilted propagation on the left, with typical side view in the propagation axis. Plate initial thickness is 25.4 mm. Left part of the Figure shows the result of an FEM simulation of fracture of a large plate with code ZEBULON. The upper part shows a  $\frac{3}{4}$  view of the region of the plate ahead of the notch. The tip of the notch can be seen on the right end. The quadrangular mesh is shown. Gray-scale code corresponds to void volume fraction. Light meshes are completely ruined. Gray meshes are sound. Dark meshes mean intermediate damage. The bottom pictures provide 8 cuts showing the crack tilting: on the left, at the onset of propagation, the crack is almost flat. It progressively tilts to be fully  $45^\circ$  oriented by the 4<sup>th</sup> bottom picture (from the right).

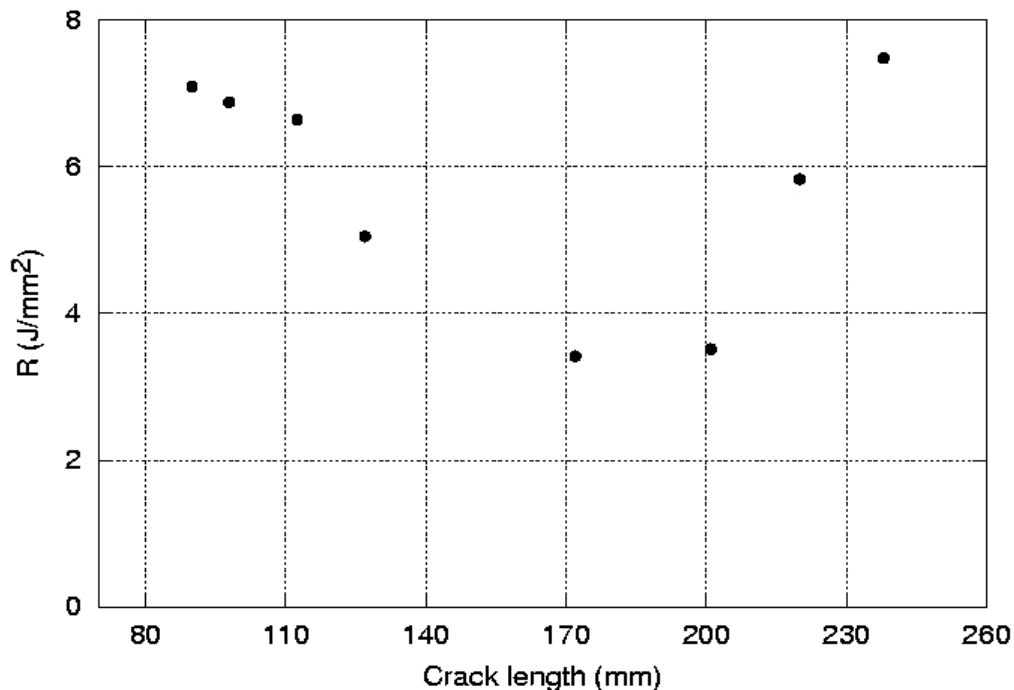


Fig.10: Energy dissipation rate  $R$  as a function of crack advance on 20 mm thick X100 steel. Union of small scale testing and large scale testing provides data to set a complete simulation

procedure. Indeed, model parameters issued in the first place from small scale fracture testing are then adapted to recover the results of the large scale testing; mainly temperature dependency is introduced at the latter stage.

The data are in course of implementation in FEM code ZEBULON developed at Ecole Nationale Supérieure des Mines de Paris. To show the capability of this procedure, Figure 9 also presents (on the right) a numerical simulation (performed for Aluminium) representative of a crack tilting around its propagation axis.

## 6. LONG DISTANCE RUNNING CRACK AND REMESHING METHODOLOGY

As explained above, fracture FEM simulation relying on local approach to ductile fracture requires the use of very fine mesh, typically  $(0.2 \text{ mm})^3$ . On that basis, one easily finds that the total fracture zone of a dynamic testing specimen (Figure 3) would contain around 10 million meshes; that of a 20 meter long pipe rupture would contain around 1 billion meshes. Because such a computation size is not yet achievable, one can use remeshing to use a fine grid mesh in the fracture zones only at the time when fracture is in process at that point.

The first track which can be considered is frequent automatic remeshing governed by fracture computation itself. This leads to a random mesh and it is known to be possible only for tetrahedron meshes. Because plastic flow is almost incompressible, this forces to develop specially enriched tetragonal elements, as explained in [12]. This approach should allow to follow with precision the crack three-dimensional geometry. Because fracture model shows localising properties, it appears that computation time steps with remeshing should not be too frequent, otherwise they could generate artificial damage parameter diffusion and smear out fracture specificity [12].

The second track is to take advantage of the fact that fracture path is not completely random, and to use an organized remeshing algorithm which sets barriers to artificial damage diffusion. Firstly, any zone of the simulation undergoes two (possibly void) stages: (i) a refining stage, and then: (ii) a coarsening stage. Secondly, any refined mesh follows the boundary of its parent coarser mesh, with no damage diffusion outside of it. Thirdly, during active damage evolution, no mesh change is allowed. Fourthly, during coarsening, parent mesh is retrieved and there is no damage diffusion. The essential steps of this algorithm, the second and the fourth ones, are depicted on Figure 11.

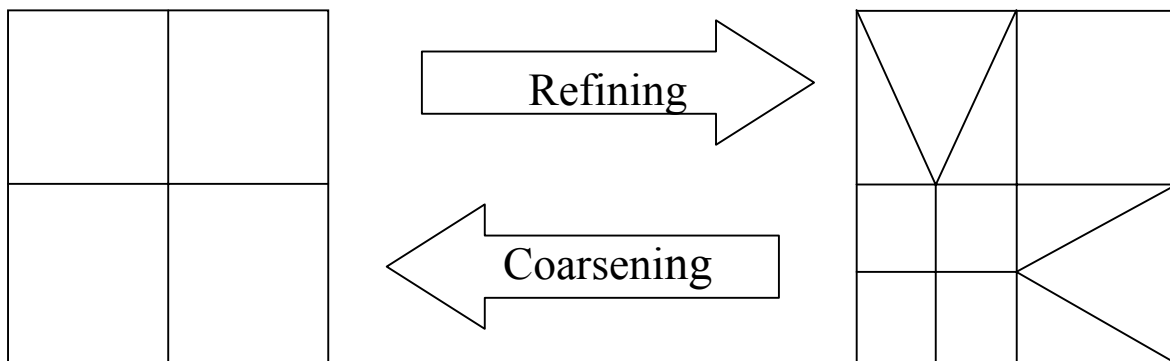


Fig. 11: Illustration of the refining and coarsening stages of the organized remeshing algorithm.

## 7. CONCLUSION

In order to define an adequate assessment procedure for crack propagation arrest from some in-mill acceptance test, adapted to X100 steel, understanding fast axial ductile gas pipeline fracture and quantify is important.

The present study is focused on a precise steel: X100 steel provided by EUROPIPE. However, the authors believe that the developed methodology can be helpful for addressing similar issues for any TMCP bainitic steel of grade X90 through X120.

One of the few problems preventing use of X100 steel for gas pipelines is the hiatus between present Charpy-like, fracture oriented in-mill acceptance tests and scale 1 burst results. Because crack propagation is tortured and tilted instead of flat, FEM simulation models used to bridge this hiatus should be fully 3D, based on some Gurson inspired model. Small scale and large scale testing are used. Development of a meshing strategy based on nested remeshing zones is also needed.

Scale 1 burst context will be adequate for testing the above hypothesis, according to which essential aspects of behaviour law should be unchanged when changing crack velocity range from 20 m/s to 200 m/s. Also, it reinforces the interest of dynamic meshing technique for crack propagation simulation.

To simulate scale 1 burst tests, coupling the fracture mechanics simulation tool presented with other programs which simulate other key phenomena is also necessary (gas pressure simulation, flap opening, soil mechanics for an underground pipe).

These issues are left for future work, a part of which will be treated from late 2005 to 2007 in an IFP led Joint Industry Project (see [11]).

## ACKNOWLEDGEMENTS

The authors wish to thank Jean-Pierre Jansen (EUROPIPE), Stéphane Hertz-Clémens (Gaz de France) and Henri Godinot (TOTAL) for active and financial support.

## REFERENCES

- [1] BECKER, R, NEEDLEMAN, A, RICHMOND, O AND TVERGAARD, V (1988). "Void Growth and Failure in Notched Bars", *J. Mech. Phys. Solids*. Vol. 36, pp. 317.
- [2] BRON, F and BESSON, J (2004). "A yield function for anisotropic materials – Application to aluminum alloys", *Int. J. Plasticity*, vol. 20, pp. 937-963.
- [3] BUZZICHELLI, G (2000). "Designing Against Ductile Fracture Propagation in High Strength Steel Gas Pipelines: a Review", *Fracture Mechanics: Applications and Challenges*, Eds. M. Fuentes, M. Elices, A. Martin-Meizoso and J.M. Martinez-Esnaola, ESIS publication 26.
- [4] GURSON AL (1977). "Continuum Theory of Ductile Rupture by Void Nucleation and Growth : Part I – Yield Criteria and Flow Rules for Porous Ductile Media", *J. Eng. Mater. Technol.*, Vol. 99, pp. 2-15.

- [5] KANNINEN, MF, MORROW, TB, GRAT, TS and DEMOFONTI, G. (1994) "The development and validation of a ductile fracture analysis model", *Final report, SwRI Poject No. 07-5007*.
- [6] KOPLIK, J AND NEEDLEMAN, A (1988). "Void Growth and Coalescence in Plastic Solids", *Int. J. Solids Struct.* Vol. 24, pp. 835.
- [7] LUU, TT (2005). "Approche locale de la déchirure des aciers modernes, à haute limite d'élasticité - Application aux gzoducs", *Rapport à mi-thèse de l'Ecole Nationale Supérieure des Mines de Paris*.
- [8] MARINI, B, MUDRY, F AND PINEAU, A (1985). "Experimental Study of Cavity Growth in Ductile Rupture", *Eng. Frac. Mech.*, Vol. 22, pp. 989-996.
- [9] MAXEY, WA (1981). "Dynamic Crack Propagation in Line Pipe" in *Analytical and Experimental Fracture Mechanics*, Sih, GC and Mirabile M, eds., pp. 109-123, Rome.
- [10] MC CLINTOCK, FA (1971). "Plasticity aspects of Fracture" in *Fracture* Liebowitz, H. , ed.. Vol. 3, pp. 47-225.
- [11] PERRIN, G (2005). "CharpyX100 JIP", [www.ifp.fr](http://www.ifp.fr).
- [12] PERRIN, G, MARTINEZ, M, ODRU, P, LUU, T, PINEAU, A, TANGUY, B and BESSON, J (2005). "Towards X100 gas pipes assessment against propagating axial crack hazard", *ISOPE 2005, Seoul*.
- [13] RIVALIN, F, PINEAU, A, DI FANT, M and BESSON, J (2001). "Ductile tearing of pipeline-steel wide plates I. Dynamic and quasi-static experiments", *Engineering Fracture Mechanics*, 68 pp. 329-345.
- [14] RIVALIN, F, PINEAU, A, DI FANT, M and BESSON, J (2001). "Ductile tearing of pipeline-steel wide plates II. Modeling of in-plane crack propagation", *Engineering Fracture Mechanics*, 68 pp. 347-364.